doi: 10.4149/gpb_2015015

Biophysical characterization of inwardly rectifying potassium currents (I_{K1}, $I_{K,ACh}$, $I_{K,Ca}$) using sinus rhythm or atrial fibrillation action potential waveforms

Chuyi Tang[1,2], Lasse Skibsbye[2], Lei Yuan[2], Bo H. Bentzen[2] and Thomas Jespersen[2]

[1] *Department of Cardiovascular Medicine, East Hospital, Tongji University School of Medicine, No. 150, Jimo Rd. Shanghai, China*

[2] *Danish Arrhythmia Research Centre, Department of Biomedical Sciences, Faculty of Health Sciences, University of Copenhagen, Denmark*

Abstract. Although several physiological, pathophysiological and regulatory properties of classical inward rectifier K^+ current I_{K1}, G-protein coupled inwardly-rectifying K^+ current $I_{K,ACh}$ and the small-conductance Ca^{2+} activated K^+ current $I_{K,Ca}$ have been identified, quantitative biophysical details remain unclear. Both I_{K1} and $I_{K,ACh}$ are implicated in atrial fibrillation (AF), and recently also $I_{K,Ca}$ has been speculated to be linked with the genesis and sustainability of AF. All these three currents have been shown to be involved in the electrical remodeling in the atria of patients suffering from AF, and it is therefore important to characterize their biophysical properties and compare their relative current contribution in atrial electrophysiology in both sinus rhythm (SR) and AF. The aim of this study is to investigate the contribution of the three potassium currents when subjected to voltage protocols adapted from atrial action potentials recorded in human tissue at 1 and 3 Hz. The current recordings were performed in the HEK-293 heterologous cell system expressing either I_{K1}, $I_{K,ACh}$ or $I_{K,Ca}$ to establish the individual contribution of each of these currents during the voltage changes of atrial action potential waveforms. I_{K1} primarily contributes to the atrial electrophysiology at the latter part of repolarization and during the diastolic phase, while both $I_{K,Ca}$ under high $[Ca^{2+}]_i$ and $I_{K,ACh}$ contribute relatively most during repolarization.

Key words: Inwardly rectifying potassium channel — Small-conductance calcium-activated potassium channel — Action potential-voltage clamp — Atrial fibrillation

Abbreviations: ACh, acetylcholine; AF, atrial fibrillation; AP, action potential; CaM, calmodulin; GIRK current, G-protein coupled inwardly rectifying potassium current; RMP, resting membrane potential; SR, sinus rhythm.

Introduction

The cardiac action potential (AP) is formed by depolarizing Na^+ and Ca^{2+} currents and repolarizing K^+ currents. A number of different types of potassium channels are known to play important roles in both shaping the cardiac AP and in controlling the diastolic potential, referred to as the resting membrane potential (RMP). The voltage-gated K^+ channels Kv1.5 (I_{Kur}), Kv4.3 (I_{to}), Kv11.1 (I_{Kr}) and Kv7.1 (I_{Ks}), are important in conducting K^+ current both in the early (I_{Kur}, I_{to}) and late (I_{Kr}, I_{Ks}) phase of repolarization (Nerbonne and Kass 2005). However, the voltage independent inwardly rectifying K^+ channels Kir2.1 (I_{K1}), Kir3.1/Kir3.4 ($I_{K,ACh}$) and small-conductance Ca^{2+} activated K^+ channel SK/K_{Ca}2.X ($I_{K,Ca}$) are also very important in shaping the AP and at the same time these currents play a crucial role in setting RMP (Lopatin and Nichols 2001; Nerbonne and Kass 2005; Grunnet et al. 2012; Skibsbye et al. 2014).

Correspondence to: Thomas Jespersen, Danish Arrhythmia Research Centre, Department of Biomedical Sciences, Faculty of Health Sciences 16.5.20. Blegdamsvej 3B, DK-2200, Copenhagen, Denmark
E-mail: thojes@sund.ku.dk

Kir2.1, Kir2.2, and Kir2.3 proteins underlie cardiac I_{K1}, and Kir2.1 is found to be the most abundant in the human heart (Liu et al. 2001). I_{K1} is absent in nodal tissue, present in atria and prominently expressed in ventricles and Purkinje system (Varro et al. 1993). I_{K1} shows a strong inward rectification at positive membrane potentials due to blockage by polyamines and divalent cations, such as Mg^{2+} and Ca^{2+} (Fakler et al. 1995). In addition, the conductance and rectification of I_{K1} also depends on the extracellular K^+ concentration (Panama and Lopatin 2006).

Heteromeric assembly of Kir3.1 and Kir3.4 subunits underlie the G-protein coupled inwardly rectifying potassium (GIRK) current $I_{K,ACh}$ (Krapivinsky et al. 1995). $I_{K,ACh}$ channels are regulated by βγ subunits of G_i/G_o-coupled receptors. G-protein coupled receptors activated by acetylcholine (ACh), (muscarinic M2 receptors) and adenosine (adenosine 1 receptors) (Kofuji et al. 1995; Wang et al. 2013; Liang et al. 2014) have been shown to increase $I_{K,ACh}$ activity in the atrial myocytes, suggesting that $I_{K,ACh}$ may play a functional role in the atria both when the heart is at rest (vagal release of ACh) and during work or cellular stress (local release of adenosine). $I_{K,ACh}$ is primarily expressed in the atria and nodal tissue (Noma and Trautwein 1978; Sakmann et al. 1983) and rectifies to a much weaker extent than I_{K1} (Makary et al. 2005).

Small-conductance calcium-activated potassium (SK) channels play an important role in afterhyperpolarization of neuronal APs, but are also found expressed in many other tissues, including the heart (Lancaster et al. 1991; Tse and Hille 1992; Grissmer et al. 1993; Pribnow et al. 1999; Xu et al. 2003). In the mammalian heart, SK channels are formed by homomeric and heteromeric complexes of SK1, SK2 and SK3 proteins (Tuteja et al. 2010). Calmodulin (CaM), which is constitutively bound to the calmodulin-binding-domain at the C-terminal of each SK channel subunit, serves as a Ca^{2+} sensor (Maylie et al. 2004). SK channels are rapidly responding and highly sensitive to intracellular Ca^{2+} ($K_{0.5}$ = 0.3–0.7 μmol/l, Hill coefficient = 3–5) (Hirschberg et al. 1998; Stocker 2004). At positive membrane potentials, Ca^{2+} not only activates, but also blocks SK channels in a concentration-dependent manner, giving rise to a moderate inwardly rectifying K^+ current (Kohler et al. 1996; Soh and Park 2001). In the heart $I_{K,Ca}$ participates in the electrophysiology of the atria. Pharmacological blockage of these channels prolongs AP duration and refractory period, and has shown antiarrhythmic potential in experimental models of atrial fibrillation (Diness et al. 2010, 2011; Skibsbye et al. 2011, 2014).

In this study we have measured currents I_{K1}, $I_{K,Ach}$ and $I_{K,Ca}$ using AP voltage recordings from atrial tissue obtained from patients in either sinus rhythm or persistent atrial fibrillation.

Materials and Methods

Cell lines preparation

I_{K1} and $I_{K,ACh}$ currents were investigated in transiently transfected HEK-293 and $I_{K,Ca}$ currents were studied in a pIRESpuro-hSK3 stably expressed HEK-293 cell line (Strøbæk et al. 2004). Both cell lines were kindly provided by Acesion Pharma (Copenhagen, Denmark), and were grown in Dulbecco's modified Eagle's medium (DMEM; Life Technology, NY, USA) supplemented with 10% fetal bovine serum (FBS; Sigma-Aldrich, St. Louis, USA) and 1% streptomycin (Invitrogen, Naerum, Denmark) at 37°C in a 5% CO_2 atmosphere. The stably transfected pIRESpuro-hSK3 -HEK-293 cells were selected with 100 μg/ml Geneticin (Sigma-Aldrich, St. Louis, USA).

Molecular cloning and transfection

Complementary DNAs encoding human Kir2.1 (GenBank ACC. NM_000891), human Kir3.1 (GenBank ACC. NM_002239) and human Kir3.4 (GenBank ACC. NM_000890) were subcloned into pcDNA3 or pXOOM (Yang et al. 2010).

To reconstitute I_{K1} currents HEK-293 cells were transiently transfected with 1 μg pXOOM-hKir2.1 and 0.2 μg pcDNA3-eGFP (reporter gene). With regard to $I_{K,ACh}$, 0.6 μg pcDNA3-hKir3.1, 0.6 μg pcDNA3-hKir3.4, 0.6 μg pcDNA3-hM2, and 0.2 μg pcDNA3-eGFP were transiently transfected into HEK-293 cells. Transfections were performed using Lipofectamine 2000 (Invitrogen, Naerum, Denmark) according to the manufacturer's instructions. The cells were used for patch-clamp recordings 36 to 48 hours after transfection.

Solutions and chemicals

The following physiological extracellular solutions were used for the electrophysiological experiments, containing (in mmol/l): NaCl 140, KCl 4, $CaCl_2$ 2, $MgCl_2$ 1, HEPES 10, D-glucose 10 (pH 7.4 with NaOH). The internal pipette solution for I_{K1}, $I_{K,ACh}$ measurements consisted of (in mmol/l) KCl 140, Na_2ATP 1, EGTA 2, HEPES 10, $CaCl_2$ 0.1, $MgCl_2$ 1, D-glucose 10 (pH 7.4 with KOH). For $I_{K,Ca}$ recording, pipettes were filled with solutions containing (in mmol/l): KCl 144, EGTA 10 or 1, nitrilotetraacetic acid (NTA) 0 or 9, and HEPES 10 (pH 7.2 with KOH). $CaCl_2$ and $MgCl_2$ were added in concentrations calculated (EqCal; BioSoft, Cambridge, UK) to give a free Mg^{2+} concentration of 1 mmol/l and free Ca2+ concentrations of either 0.1 or 1 μmol/l, respectively (Grunnet et al. 2001). 100 nmol/l of apamin (Alomone Labs, Jerusalem, Israel) was added to the perfusate to block $I_{K,Ca}$ currents. $I_{K,ACh}$ currents were identified in the presence of

extracellular ACh combined with 20 nmol/l Tertiapin-Q (TTQ) (Alomone Labs, Jerusalem, Israel) blockage. Solutions containing ACh, apamin and TTQ, respectively, were freshly prepared prior to each experiment.

Electrophysiological methods

Patch-clamp recordings were performed as previously described (Grunnet et al. 2001; Yuan et al. 2014). HEK-293 cells were voltage-clamped with either ramp or AP-shaped protocols. The AP waveform protocols were recorded using microelectrode impalement of multicellular muscle preparations at 1 Hz and 3 Hz of electric stimulation frequency in human right atrial appendages trabeculae muscle from sinus rhythm (SR) or chronic atrial fibrillation (AF) patients (Skibsbye et al. 2014), and were subsequently used as voltage command by programming into a Pulse Generator File (PGF). Whole-cell currents were measured at room temperature (20–22°C) with an EPC-9 amplifier and Pulse software (both from HEKA Elektronik, Lambrecht, Germany). Borosilicate glass pipettes were pulled on a DPZ-Universal puller (Zeitz Instrumente, Munich, Germany). The pipettes had a resistance of 1.5–2.5 MΩ. The series resistances for whole-cell configuration were 2–5 MΩ and were 80% compensated. At least 1.0 GΩ were achieved in all experiments.

Data analysis

Illustration was drawn with Adobe Illustrator software (Adobe Systems, San Jose, USA). Statistical analyses were performed using IGOR Pro (WaveMetrics, Lake Oswego, USA) and GraphPad Prism software (GraphPad Software, San Diego, USA). All AP voltage command parameters were obtained as an average of > 10 APs. Data are presented as mean ± SEM. The authors had full access to the data and take responsibility for its integrity.

Results

I_{K1}, $I_{K,ACh}$ and $I_{K,Ca}$ are known to play prominent roles in atrial electrophysiology (Fig. 1A). However, the relative contributions of these currents during the different phases of the atrial AP have not been thoroughly addressed. In this study we use atrial AP voltage recordings obtained by sharp microelectrode measurements in freshly isolated human tissue (Fig. 1B) (Skibsbye et al. 2014). These recordings were used as voltage command protocols with the patch-clamp technique on HEK-293 cells transiently transfected with either Kir2.1 or Kir3.1/Kir3.4/M2, or stably expressing hSK3, recapitulated the inwardly rectifying currents I_{K1}, $I_{K,ACh}$ and $I_{K,Ca}$, respectively. Two kinds of protocols were applied: 1000 ms voltage ramp protocol from –120 mV to 60 mV, and AP voltage command waveforms recorded at a 1 and 3 Hz pacing frequency on human right atrial trabeculae muscle from SR or chronic AF patients (Skibsbye et al. 2014).

Endogenous currents in HEK-293 cells during AP voltage-clamp

HEK-293 cells, like all other experimental cell systems, exhibit endogenous ionic currents (Thomas and Smart 2005). Hence, our investigations were initiated by measuring endogenous currents under the given voltage-clamp protocols on non-transfected HEK-293 cells (Fig. 2A). Currents elicited following the ramp protocol reveal a reversal potential around –30 mV, indicating endogenous expression of both repolarizing and depolarizing ionic currents. A significant outward current at positive voltages was observed, with a peak value of 21.4 ± 2.3 pA/pF at +60 mV, primarily conducted by a voltage-dependent potassium (K_v)-like current (data not shown) as also reported in (Jiang et al. 2002). When applying the AP voltage command protocols, only small currents were recorded (Fig. 2A, right panel). During the latter part of the APs and during the diastolic interval, the sum of these currents was negative due to the relatively depolarized reversal potential (≈ –30 mV).

I_{K1} (Kir2.1)

I_{K1} currents recorded by ramp and AP voltage commands after subtracting endogenous currents are shown in Fig. 2B. In agreement with previous studies, I_{K1} is a strong inward rectifier, with high inward conduction at potentials negative to the reversal potential (–85.6 ± 3.2 mV), and prominent outward conduction between –60 and –80 mV. When comparing the I_{K1} current levels at 50% and 90% of the repolarization of the AP (APD_{50} and APD_{90}, respectively), it is found that at $APD_{50,}$ I_{K1} only conducts 8% (SR) and 13% (AF) as compared to the I_{K1} current conducted in the diastolic interval, while this number is 66% (SR) and 76% (AF) at APD_{90} (Table 1). This clearly demonstrates that I_{K1} primarily contributes to the atrial electrophysiology in the very late part of the AP and during the diastolic interval.

$I_{K,ACh}$ (Kir3.1/3.4)

By applying the $I_{K,ACh}$ specific blocker Tertiapin Q (TTQ), acetylcholine-stimulated $I_{K,ACh}$ currents could be calculated by subtraction (averaged TTQ sensitive currents shown in Fig 3). $I_{K,ACh}$ rectifies to a much lesser extent than I_{K1}. Positive to the membrane reversal potential around –82.6 ± 1.2 mV, the outward currents of $I_{K,ACh}$ slowly increases following depolarization, giving an almost similar outward current level from –30 mV to 60 mV. This results in cur-

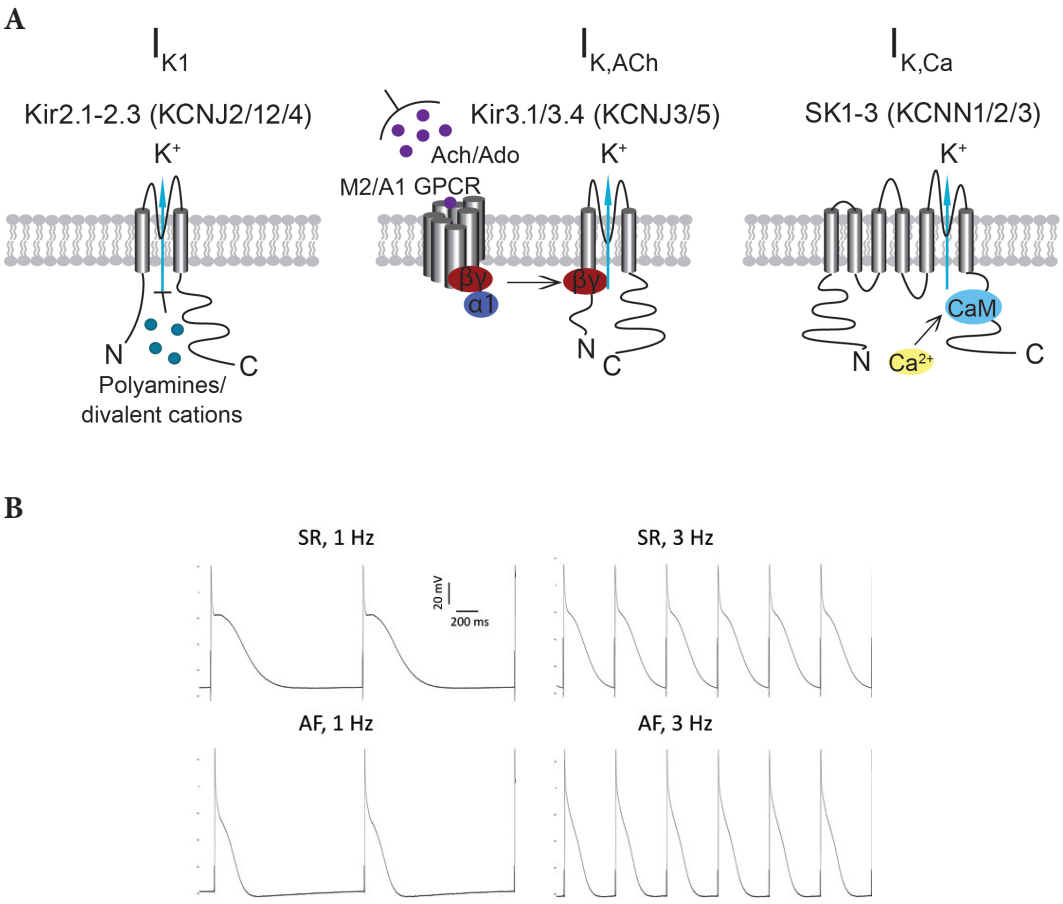

Figure 1. Topology of inward rectifying channels and human atrial AP recordings **A.** Topology of the α-subunits forming the three potassium channels. These three channels are assembled into tetrameric complexes to form functional channels. Left and middle, schematic representation of Kir channels, holding two transmembrane domains connected by a pore forming loop. For $I_{K,ACh}$ channels, G-protein coupled receptors are activated by acetylcholine (Ach; muscarinic 2 receptor) and adenosine (Ado; adenosine 1 receptor). Right, SK channel subunits contain six transmembrane domains and a pore loop, with intracellular N and C termini. Calmodulin (CaM) binds to the proximal domain of the C terminus, mediating Ca^{2+} activation. **B.** Representative AP potential recordings from trabeculae muscle strips removed from patients either in sinus rhythm (SR) or permanent atrial fibrillation (AF) (more than 6 months), impaled with a sharp electrode and paced at either 1 Hz or 3 Hz (these recordings constitute a part of the dataset published in Skibsbye et al. (2014).

rents being larger during AP repolarization than during the diastolic interval, because the driving force for K^+ efflux is larger. For the same reason, the 6 mV difference between SR and AF during the diastolic interval (–74 mV *vs.* –80 mV) leads to a robust decrease of the diastolic $I_{K,ACh}$ current in the AF-setting, compared with that in SR. As a consequence, the relative contribution of $I_{K,ACh}$ during both the early and the latter part of the AP is prominent (Table 1).

$I_{K,Ca}$ (SK3)

In cardiomocytes, the dynamic changes of $[Ca^{2+}]_i$ during systole and diastole range approximately between 0.1 µmol/l and 1.0 µmol/l (Beuckelmann et al. 1992; Eisner 2014). As it is not possible for HEK-293 cells to fabricate the dynamic changes in $[Ca^{2+}]_i$ as cardiomyocytes during excitation and contraction, we investigated $I_{K,Ca}$ with clamped $[Ca^{2+}]_i$ at 0.1 µmol/l and 1.0 µmol/l, respectively (see "Materials and Methods") (representative traces Fig. 4A). To isolate the specific SK channel currents we applied the highly selective SK channel blocker apamin (100 nmol/l). With 1.0 µmol/l $[Ca^{2+}]_i$ $I_{K,Ca}$ shows a weak inward rectifier current. The amount of 0.1 µmol/l $[Ca^{2+}]_i$ did not, as reported by others, evoke specific $I_{K,Ca}$ (Romey and Lazdunski 1984). In Fig. 4B average apamin sensitive currents with 1.0 µmol/l $[Ca^{2+}]_i$ are shown. As revealed by the ramp protocol, due to the low degree of rectification the current is much higher around 0 mV than at potentials

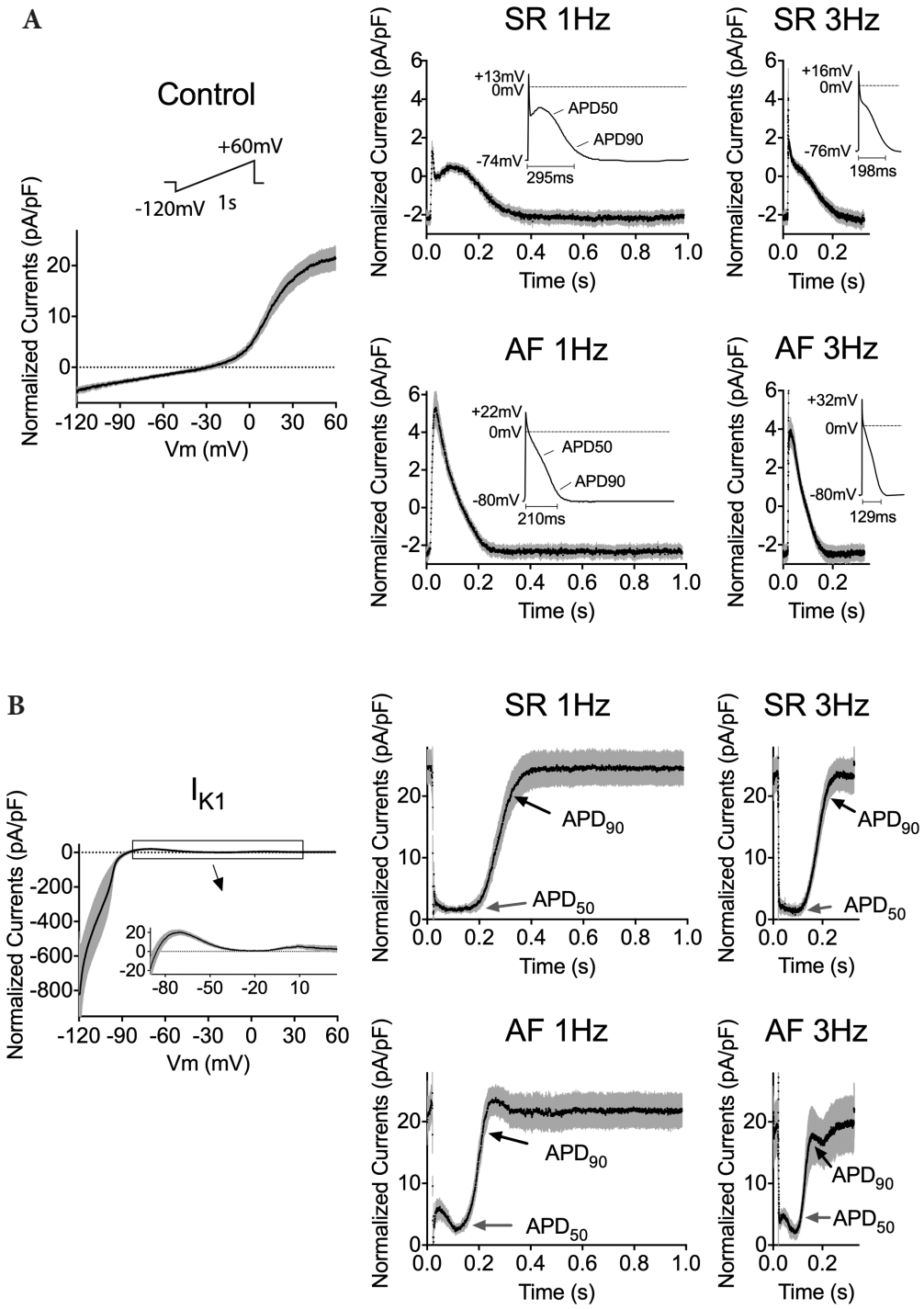

Figure 2. Endogenous and I_{K1} current recorded following ramp and human atrial action potential voltage commands. **A.** Recordings show endogenous currents elicited by ramp and action potential (AP) voltage-clamp protocols. The outer boundary of the grey shading illustrates SEM. Left, current recorded during 1000 ms voltage ramp from –120 mV to 60 mV from a holding potential of –74 mV (insert at top). Right, recordings show naïve HEK cell membrane currents produced by AP-shaped voltage-clamp protocols (inserted at right top of each graph). Action potential durations at 90% repolarization (APD_{90}) and at 50% repolarization (APD_{50}) indicated in the traces of AP-shaped protocols. The time values of APD_{90} shown below the protocol traces. Dotted lines indicate 0 pA/pF; Vm indicates membrane voltage; n = 10 in each group. **B.** I_{K1} currents expressed in HEK-293 cells following ramp and human AP voltage commands after subtraction of the endogenous currents recorded in A. In the ramp protocol current between –80 mV and –35 mV is enlarged. n = 4 in each group. SR, sinus rhythm; AF, atrial fibrillation.

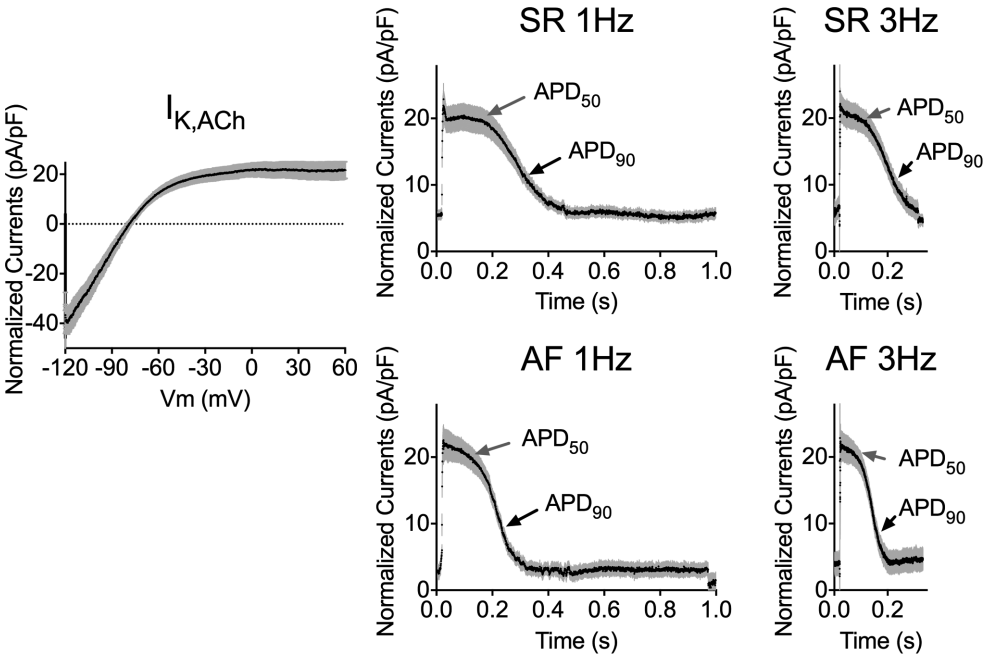

Figure 3. $I_{K,ACh}$ current recorded following ramp and human atrial action potential voltage commands. TTQ sensitive currents are shown. Vm indicates membrane voltage; $n = 9$ in each group. (For abbreviations, see Fig. 2).

close to the diastolic potentials. This is reflected in the AP voltage command recordings. Under these experimental conditions we observed an outward diastolic current, significantly larger in SR than AF. This is a consequence of the hyperpolarized diastolic potential in AF. Interestingly, during the latter part of the APs (APD_{90}), where $[Ca^{2+}]_i$ is known to be high (Bouchard et al. 1995), prominent SK currents are recorded. At APD_{50} $I_{K,Ca}$ is 10- to 12-fold higher in SR and 28- to 32-fold higher in AF than during the diastolic interval. Also at APD_{90} a ~2.5-fold higher current is found in SR and a ~4.5-fold higher current in AF as compared to diastolic current (Table 1).

Discussion

I_{K1}, $I_{K,ACh}$ and $I_{K,Ca}$ are three prominent inwardly rectifying K^+ currents involved in cardiac electrical activity. These currents are important for repolarizing the atrial cardiomyocyte AP following excitation and thereby in defining the relative refractoriness of the atria. Further, as all three currents have significant conductance at hyperpolarized potentials, they play a prominent role in setting the diastolic potential (resting membrane potential) where only minor changes in the potential has large impact on sodium channel availability, due to the steepness of the inactivation curve for $Na_v1.5$

Table 1. Systolic and diastolic current ratios. Relative current ratios at 50% (APD_{50}) and 90% (APD_{90}) action potential duration compared to the diastolic interval current, at 1 Hz and 3 Hz, respectively

Systolic/diastolic current		1 Hz			3 Hz		
		I_{K1}	$I_{K,ACh}$	$I_{K,Ca}$*	I_{K1}	$I_{K,ACh}$	$I_{K,Ca}$*
APD50	SR	0.08	3.7	9.8	0.06	3.2	12
	AF	0.13	6.3	28	0.21	5.1	32
APD90	SR	0.66	2.0	2.5	0.73	1.7	2.7
	AF	0.76	2.7	4.5	0.53	2.2	5.0

* $I_{K,Ca}$ evoked with 1 μmol/l intracellular Ca^{2+}; I_{K1}, classical inward rectifier K^+ current; $I_{K,ACh}$, G-protein coupled inwardly-rectifying K^+ current; $I_{K,Ca}$, small-conductance Ca^{2+} activated K^+ current; APD_{50}, 50% of the repolarization of the action potential; APD_{90}, 90% of the repolarization of the action potential; SR, sinus rhythm; AF, atrial fibrillation. 1 Hz: Pulse protocol (PGF) derived from action potential generated at 1 Hz electric stimulation; 3 Hz: PGF derived from action potential generated at 3 Hz electric stimulation.

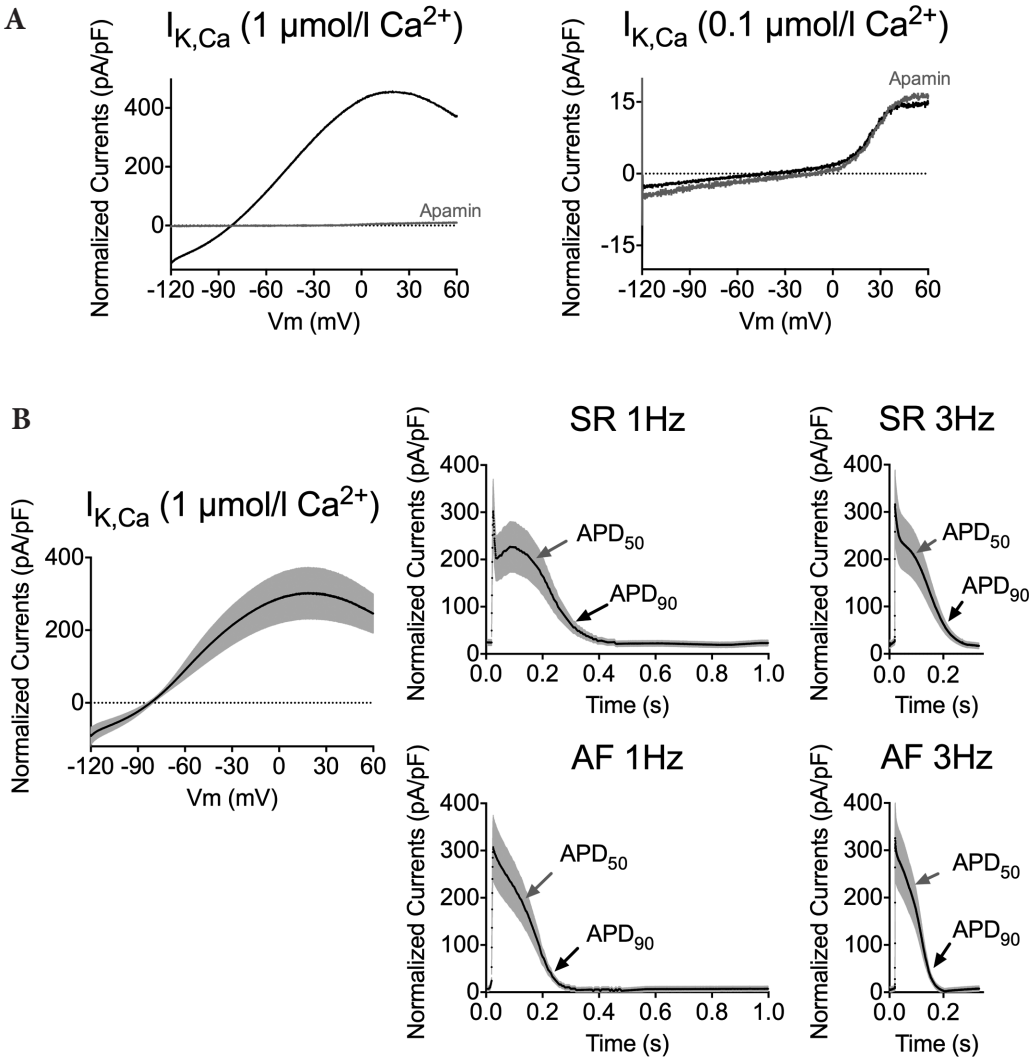

Figure 4. $I_{K,Ca}$ current recorded following ramp and human atrial action potential voltage commands. **A.** Representative $I_{K,Ca}$ currents evoked with either 1 or 0.1 µmol/l intracellular Ca^{2+}. SK currents were following blocked by apamin (gray traces). **B.** Apamin sensitive currents recorded in HEK-293 cells with 1.0 µmol/l intracellular Ca^{2+}. Vm indicates membrane voltage; $n = 10$ in each group. (For abbreviations, see Fig. 2).

channels at these voltages. Such changes in sodium channel availability will mediate huge impact on cellular refractoriness and secondarily influence the conduction of the AP throughout the atria. We have in this study measured I_{K1}, $I_{K,ACh}$ and $I_{K,Ca}$ currents separately following SR or AF AP voltage-clamping and thereby obtained new information concerning the relative contribution of potassium currents during the different phases of the human atrial AP.

Inward rectifier K^+ currents

Inward rectifier potassium channels are fundamentally different from voltage-gated (K_v) channels, as they have the biophysical property of favouring influx of K^+ ions at potentials negative to the reversal potential, while the outward current is relatively reduced (non linear in respect to driving force) at depolarized potentials. The voltage-dependence of the channels lies in a physical occlusion of the channel pore by depolarization-induced motion of intracellular cations, such as polyamines and Mg^{2+}. In fact, I_{K1} and $I_{K,ACh}$ are two out of seven subfamilies showing classical strong rectification (Anumonwo and Lopatin 2010). The channel complexes conducting these two currents have been suggested to mainly contribute to the late part of the AP and in balancing the diastolic potential (Lopatin and Nichols 2001; Anumonwo and Lopatin 2010). However, our study indicates that $I_{K,ACh}$

actually contributes profoundly during the whole action potential, including the plateau phase. This is due to the relatively weak inward rectification of $I_{K,ACh}$ as compared to I_{K1} (Bender et al. 2001). In contrast, I_{K1} conducts almost zero current at potentials positive to –60 mV. Thus, the functional impact of I_{K1} and $I_{K,ACh}$ is very different as $I_{K,ACh}$ will conduct current at all potentials, including the most depolarized part of the AP, while the strong rectification of I_{K1} ensures conduction of K^+ ions only at potentials close to the resting membrane potential. This implies that G_i receptor activation of $I_{K,ACh}$, such as during vagal stimulation of muscarinic 2 receptors (Kofuji et al. 1995) or exercise/ischemia-dependent activation of adenosine 1 receptors (Wang et al. 2013; Liang et al. 2014), will result in an AP duration shortening, and a hyperpolarization of the diastolic potential.

In patients with AF the atria undergo electrical remodelling whereby the relative functionality of a number of atrial ion channels is altered. I_{K1} has been shown to be upregulated in AF (Van Wagoner et al. 1997; Bosch et al. 1999; Workman et al. 2001), and suggested to be the major contributing factor for the ~6 mV hyperpolarization of the diastolic potential. Pathophysiological conditions have also been reported to take part in the regulation and remodelling of $I_{K,Ach}$ (Zhao et al. 2009; Voigt et al. 2010). As shown here, $I_{K,Ach}$ currents conduct during the entire AP. The acetylcholine-activated current is found to be down-regulated in AF (Dobrev et al. 2001, 2002), while the constitutively active component of $I_{K,ACh}$ is upregulated (Dobrev et al. 2005). The augmentation of I_{K1} and constitutively active component of $I_{K,ACh}$ is believed to underly a significant part of the shortening of APD and effective refractory period observed in AF tissue. The relative contribution of the inward rectifying currents was not different between 1 and 3 Hz. This is due to the biophysical properties of these channels, responding instantaneously to changes in voltage potential.

Role of $I_{K,Ca}$ in AP forming

We have used a heterologous expression system clamped with a low (0.1 µmol/l) and high (1.0 µmol/l) intracellular free calcium concentration. During the cardiac action potential a fast increase in global intracellular calcium, reaching up to 1 µmol/l, which lasts until the end of the AP, is observed in cardiomyocytes (Beuckelmann et al. 1992; Bouchard et al. 1995). As SK channel activation is strictly dependent on rises in intracellular free calcium, it is questionable whether SK channels are conducting throughout the diastolic interval when the atria are beating in sinus rhythm. In contrast, during AF the intracellular calcium dynamics and Ca^{2+} handling is compromised and the exact mechanisms of Ca^{2+} signalling in space and time remain unravelled. In this regard, AF could be hypothesized to give rise to a reduced clearing of intracellular Ca^{2+} in the fibrillating atria, which potentially would lead to a constitutive activation of $I_{K,Ca}$. Further, the exact association and dissociation constants for binding of Ca^{2+} to calmodulin, which is attached to SK channels and essential for its activation, have not been elucidated in normal or diseased cardiomyocytes. However, in pyramidal neurons it has been reported that SK channels mediate intermediate afterhyperpolarization lasting hundreds of milliseconds (Stocker 2004). Hence, when interpreting our results it is important to keep in mind that we have not included the calcium dynamics found in intact cardiomyocytes.

We find that activated $I_{K,Ca}$ has a large outward K^+ current throughout the AP protocol. Hence, our results reveal that $I_{K,Ca}$ is not only of importance in the late part of the AP repolarization and in the early part of the diastolic interval, but could potentially also contribute significantly during earlier stages of the AP from when $[Ca^{2+}]_i$ is increased above the diastolic level (Beuckelmann et al. 1992; Bouchard et al. 1995).

In conclusion, we have analyzed the potassium current contribution of I_{K1}, $I_{K,ACh}$ and $I_{K,Ca}$ when subjected to voltage protocols adapted from atrial action potentials recorded in human tissue at 1 and 3 Hz both from SR patients and electrically remodeled AF patients. I_{K1} primarily contributes to the atrial electrophysiology at the latter part of repolarization and during the diastole phase, while our investigations suggest that both $I_{K,ACh}$ and $I_{K,Ca}$ contribute significantly to a major part of the repolarization of the AP and to a minor part of the diastolic potential.

Acknowledgments. S.C.Van Foundation, China Scholarship Council (CSC), Danish Council for Independent Research, Prof. Ursula Ravens is thanked for sharing the representative human atrial action potential recordings.

References

Anumonwo J. M., Lopatin A. N. (2010): Cardiac strong inward rectifier potassium channels. J. Mol. Cell. Cardiol. **48,** 45–54 http://dx.doi.org/10.1016/j.yjmcc.2009.08.013

Bender K., Wellner-Kienitz M. C., Inanobe A., Meyer T., Kurachi Y., Pott L. (2001): Overexpression monomeric and multimeric GIRK4 subunits in rat atrial myocytes removes fast desensitization and reduces inward rectification of muscarinic K(+) current (I(K(ACh))). Evidence for functional homomeric GIRK4 channels. J. Biol. Chem. **276,** 28873–28880 http://dx.doi.org/10.1074/jbc.M102328200

Beuckelmann D. J., Nabauer M., Erdmann E. (1992): Intracellular calcium handling in isolated ventricular myocytes from patients with terminal heart failure. Circulation **85,** 1046–1055 http://dx.doi.org/10.1161/01.CIR.85.3.1046

Bosch R. F., Zeng X., Grammer J. B., Popovic K., Mewis C., Kuhlkamp V. (1999): Ionic mechanisms of electrical remodeling in human atrial fibrillation. Cardiovasc. Res. **44,** 121–131

http://dx.doi.org/10.1016/S0008-6363(99)00178-9
Bouchard R. A., Clark R. B., Giles W. R. (1995): Effects of action potential duration on excitation-contraction coupling in rat ventricular myocytes. Action potential voltage-clamp measurements. Circ. Res. **76,** 790–801
http://dx.doi.org/10.1161/01.RES.76.5.790
Diness J. G., Sorensen U. S., Nissen J. D., Al-Shahib B., Jespersen T., Grunnet M., Hansen R. S. (2010): Inhibition of small-conductance Ca2+-activated K+ channels terminates and protects against atrial fibrillation. Circ. Arrhyth. Electrophysiol. **3,** 380390
http://dx.doi.org/10.1161/CIRCEP.110.957407
Diness J. G., Skibsbye L., Jespersen T., Bartels E. D., Sorensen U. S., Hansen R. S., Grunnet M. (2011): Effects on atrial fibrillation in aged hypertensive rats by Ca(2+)-activated K(+) channel inhibition. Hypertension **57,** 1129–1135
http://dx.doi.org/10.1161/HYPERTENSIONAHA.111.170613
Dobrev D., Graf E., Wettwer E., Himmel H. M., Hala O., Doerfel C., Christ T., Schuler S., Ravens U. (2001): Molecular basis of downregulation of G-protein-coupled inward rectifying K(+) current (I(K,ACh) in chronic human atrial fibrillation: decrease in GIRK4 mRNA correlates with reduced I(K,ACh) and muscarinic receptor-mediated shortening of action potentials. Circulation **104,** 2551–2557
http://dx.doi.org/10.1161/hc4601.099466
Dobrev D., Wettwer E., Kortner A., Knaut M., Schuler S., Ravens U. (2002): Human inward rectifier potassium channels in chronic and postoperative atrial fibrillation. Cardiovasc. Res. **54,** 397–404
http://dx.doi.org/10.1016/S0008-6363(01)00555-7
Dobrev D., Friedrich A., Voigt N., Jost N., Wettwer E., Christ T., Knaut M., Ravens U. (2005): The G protein-gated potassium current I(K,ACh) is constitutively active in patients with chronic atrial fibrillation. Circulation **112,** 3697–3706
http://dx.doi.org/10.1161/CIRCULATIONAHA.105.575332
Eisner D. (2014): Calcium in the heart: from physiology to disease. Exp. Physiol. **99,** 1273-1282.
http://dx.doi.org/10.1113/expphysiol.2013.077305
Fakler B., Brandle U., Glowatzki E., Weidemann S., Zenner H. P., Ruppersberg J. P. (1995): Strong voltage-dependent inward rectification of inward rectifier K+ channels is caused by intracellular spermine. Cell **80,** 149–154
http://dx.doi.org/10.1016/0092-8674(95)90459-X
Grissmer S., Nguyen A. N., Cahalan M. D. (1993): Calcium-activated potassium channels in resting and activated human T lymphocytes. Expression levels, calcium dependence, ion selectivity, and pharmacology. J. Gen. Physiol. **102,** 601–630
http://dx.doi.org/10.1085/jgp.102.4.601
Grunnet M., Jespersen T., Angelo K., Frøkjær-Jensen C., Klaerke D. A., Olesen S.-P., Jensen B. S. (2001): Pharmacological modulation of SK3 channels. Neuropharmacology **40,** 879–887
http://dx.doi.org/10.1016/S0028-3908(01)00028-4
Grunnet M., Bentzen B. H., Sorensen U. S., Diness J. G. (2012): Cardiac ion channels and mechanisms for protection against atrial fibrillation. Rev. Physiol. Biochem. Pharmacol. **162,** 1–58
Hirschberg B., Maylie J., Adelman J. P., Marrion N. V. (1998): Gating of recombinant small-conductance Ca-activated K+ channels by calcium. J. Gen. Physiol. **111,** 565–581
http://dx.doi.org/10.1085/jgp.111.4.565
Jiang B., Sun X., Cao K., Wang R. (2002): Endogenous Kv channels in human embryonic kidney (HEK-293) cells. Mol. Cell. Biochem. **238,** 69–79
http://dx.doi.org/10.1023/A:1019907104763
Kofuji P., Davidson N., Lester H. A. (1995): Evidence that neuronal G-protein-gated inwardly rectifying K+ channels are activated by G-beta-gamma subunits and function as heteromultimers. Proc. Natl. Acad. Sci. U.S.A. **92,** 6542–6546
http://dx.doi.org/10.1073/pnas.92.14.6542
Kohler M., Hirschberg B., Bond C. T., Kinzie J. M., Marrion N. V., Maylie J., Adelman J. P. (1996): Small-conductance, calcium-activated potassium channels from mammalian brain. Science **273,** 1709–1714
http://dx.doi.org/10.1126/science.273.5282.1709
Krapivinsky G., Gordon E. A., Wickman K., Velimirovic B., Krapivinsky L., Clapham D. E. (1995): The G-protein-gated atrial K+ channel IKACh is a heteromultimer of two inwardly rectifying K(+)-channel proteins. Nature **374,** 135–141
http://dx.doi.org/10.1038/374135a0
Lancaster B., Nicoll R. A., Perkel D. J. (1991): Calcium activates two types of potassium channels in rat hippocampal neurons in culture. J. Neurosci. **11,** 23–30
Liang B., Nissen J. D., Laursen M., Wang X., Skibsbye L., Hearing M. C., Andersen M. N., Rasmussen H. B., Wickman K., Grunnet M., Olesen S. P., Jespersen T. (2014): G-protein-coupled inward rectifier potassium current contributes to ventricular repolarization. Cardiovasc. Res. **101,** 175–184
http://dx.doi.org/10.1093/cvr/cvt240
Liu G. X., Derst C., Schlichthorl G., Heinen S., Seebohm G., Bruggemann A., Kummer W., Veh R. W., Daut J., Preisig-Muller R. (2001): Comparison of cloned Kir2 channels with native inward rectifier K+ channels from guinea-pig cardiomyocytes. J. Physiol. **532,** 115–126
http://dx.doi.org/10.1111/j.1469-7793.2001.0115g.x
Lopatin A. N., Nichols C.G. (2001): Inward rectifiers in the heart: an update on I(K1). J. Mol. Cell. Cardiol. **33,** 625–638
http://dx.doi.org/10.1006/jmcc.2001.1344
Makary S. M., Claydon T. W., Enkvetchakul D., Nichols C. G., Boyett M. R. (2005): A difference in inward rectification and polyamine block and permeation between the Kir2.1 and Kir3.1/Kir3.4 K+ channels. J. Physiol. **568,** 749–766
http://dx.doi.org/10.1113/jphysiol.2005.085746
Maylie J., Bond C. T., Herson P. S., Lee W.-S., Adelman J. P. (2004): Small conductance Ca2+-activated K+ channels and calmodulin. J. Physiol. **554,** 255–261
http://dx.doi.org/10.1113/jphysiol.2003.049072
Nerbonne J. M., Kass R. S. (2005): Molecular physiology of cardiac repolarization. Physiol. Rev. **85,** 1205–1253
http://dx.doi.org/10.1152/physrev.00002.2005
Noma A., Trautwein W. (1978): Relaxation of the ACh-induced potassium current in the rabbit sinoatrial node cell. Pflügers Arch. **377,** 193–200
http://dx.doi.org/10.1007/BF00584272
Panama B. K., Lopatin A. N. (2006): Differential polyamine sensitivity in inwardly rectifying Kir2 potassium channels. J. Physiol. **571,** 287–302
http://dx.doi.org/10.1113/jphysiol.2005.097741

Pribnow D., Johnson-Pais T., Bond C. T., Keen J., Johnson R. A., Janowsky A., Silvia C., Thayer M., Maylie J., Adelman J. P. (1999): Skeletal muscle and small-conductance calcium-activated potassium channels. Muscle Nerve **22,** 742–750 http://dx.doi.org/10.1002/(SICI)1097-4598(199906)22:6<742::AID-MUS11>3.0.CO;2-1

Romey G., Lazdunski M. (1984): The coexistence in rat muscle cells of two distinct classes of Ca2+-dependent K+ channels with different pharmacological properties and different physiological functions. Biochem. Biophys. Res. Commun. **118,** 669–674 http://dx.doi.org/10.1016/0006-291X(84)91355-X

Sakmann B., Noma A., Trautwein W. (1983): Acetylcholine activation of single muscarinic K+ channels in isolated pacemaker cells of the mammalian heart. Nature **303,** 250–253 http://dx.doi.org/10.1038/303250a0

Skibsbye L., Diness J. G., Sorensen U. S., Hansen R. S., Grunnet M. (2011): The duration of pacing-induced atrial fibrillation is reduced in vivo by inhibition of small conductance Ca(2+)-activated K(+) channels. J. Cardiovasc. Pharmacol. **57,** 672–681 http://dx.doi.org/10.1097/FJC.0b013e318217943d

Skibsbye L., Poulet C., Diness J. G., Bentzen B. H., Yuan L., Kappert U., Matschke K., Wettwer E., Ravens U., Grunnet M., Christ T., Jespersen T. (2014): Small-conductance calcium-activated potassium (SK) channels contribute to action potential repolarization in human atria. Cardiovasc. Res. **103,** 156–167 http://dx.doi.org/10.1093/cvr/cvu121

Soh H., Park C. S. (2001): Inwardly rectifying current-voltage relationship of small-conductance Ca2+-activated K+ channels rendered by intracellular divalent cation blockade. Biophys. J. **80,** 2207–2215 http://dx.doi.org/10.1016/S0006-3495(01)76193-0

Stocker M. (2004): Ca(2+)-activated K+ channels: molecular determinants and function of the SK family. Nat. Rev. Neurosci. **5,** 758–770 http://dx.doi.org/10.1038/nrn1516

Strøbæk D., Teuber L., Jørgensen T. D., Ahring P. K., Kjær K., Hansen R. S., Olesen S. P., Christophersen P., Skaaning-Jensen B. (2004): Activation of human IK and SK Ca2+-activated K+ channels by NS309 (6,7-dichloro-1H-indole-2,3-dione 3-oxime). Biochim. Biophys. Acta **1665,** 1–5 http://dx.doi.org/10.1016/j.bbamem.2004.07.006

Thomas P., Smart T. G. (2005): HEK293 cell line: a vehicle for the expression of recombinant proteins. J. Pharmacol. Toxicol. Methods **51,** 187–200 http://dx.doi.org/10.1016/j.vascn.2004.08.014

Tse A., Hille B. (1992): GnRH-induced Ca2+ oscillations and rhythmic hyperpolarizations of pituitary gonadotropes. Science **255,** 462–464 http://dx.doi.org/10.1126/science.1734523

Tuteja D., Rafizadeh S., Timofeyev V., Wang S., Zhang Z., Li N., Mateo R. K., Singapuri A., Young J. N., Knowlton A. A., Chiamvimonvat N. (2010): Cardiac small conductance Ca2+-activated K+ channel subunits form heteromultimers via the coiled-coil domains in the C termini of the channels. Circ. Res. **107,** 851–859 http://dx.doi.org/10.1161/CIRCRESAHA.109.215269

Van Wagoner D.R., Pond A.L., McCarthy P.M., Trimmer J.S., Nerbonne J.M. (1997): Outward K+ current densities and Kv1.5 expression are reduced in chronic human atrial fibrillation. Circ. Res. **80,** 772–781 http://dx.doi.org/10.1161/01.RES.80.6.772

Varro A., Nanasi P. P., Lathrop D. A. (1993): Potassium currents in isolated human atrial and ventricular cardiocytes. Acta Physiol. Scand. **149,** 133-142 http://dx.doi.org/10.1111/j.1748-1716.1993.tb09605.x

Voigt N., Makary S., Nattel S., Dobrev D. (2010): Voltage-clamp-based methods for the detection of constitutively active acetylcholine-gated I(K,ACh) channels in the diseased heart. Methods Enzymol. **484,** 653–675 http://dx.doi.org/10.1016/B978-0-12-381298-8.00032-0

Wang X., Liang B., Skibsbye L., Olesen S. P., Grunnet M., Jespersen T. (2013): GIRK channel activation via adenosine or muscarinic receptors has similar effects on rat atrial electrophysiology. J. Cardiovasc. Pharmacol. **62,** 192–198 http://dx.doi.org/10.1097/FJC.0b013e3182965221

Workman A. J., Kane K. A., Rankin A. C. (2001): The contribution of ionic currents to changes in refractoriness of human atrial myocytes associated with chronic atrial fibrillation. Cardiovasc. Res. **52,** 226–235 http://dx.doi.org/10.1016/S0008-6363(01)00380-7

Xu Y., Tuteja D., Zhang Z., Xu D., Zhang Y., Rodriguez J., Nie L., Tuxson H. R., Young J. N., Glatter K. A., Vazquez A. E., Yamoah E. N., Chiamvimonvat N. (2003): Molecular identification and functional roles of a Ca(2+)-activated K+ channel in human and mouse hearts. J. Biol. Chem. **278,** 49085–49094 http://dx.doi.org/10.1074/jbc.M307508200

Yang Y., Yang Y., Liang B., Liu J., Li J., Grunnet M., Olesen S.P., Rasmussen H.B., Ellinor P.T., Gao L., Lin X., Li L., Wang L., Xiao J., Liu Y., Liu Y., Zhang S., Liang D., Peng L., Jespersen T., Chen Y.H. (2010): Identification of a Kir3.4 mutation in congenital long QT syndrome. Am. J. Hum. Genet. **86,** 872-880 http://dx.doi.org/10.1016/j.ajhg.2010.04.017

Yuan L., Koivumaki J. T., Liang B., Lorentzen L. G., Tang C., Andersen M. N., Svendsen J. H., Tfelt-Hansen J., Maleckar M., Schmitt N., Olesen M. S., Jespersen T. (2014): Investigations of the Navbeta1b sodium channel subunit in human ventricle; functional characterization of the H162P Brugada syndrome mutant. Am. J. Physiol. Heart Circ. Physiol. **306,** H1204–1212 http://dx.doi.org/10.1152/ajpheart.00405.2013

Zhao Q. Y., Huang C. X., Jiang H., Okello E., Wang X., Tang Y. H., Li G. S. (2009): Acetylcholine-regulated K+ current remodelling in the atrium after myocardial infarction and valsartan administration. Can. J. Cardiol. **25,** e115–118 http://dx.doi.org/10.1016/S0828-282X(09)70069-8

Received: December 16, 2014
Final vetrsion accepted: April 15, 2015
First published online: May 22, 2015

doi: 10.4149/gpb_2015007

Lymph node mapping using quantum dot-labeled polymersomes

Rumiana Bakalova[1,2], Zhivko Zhelev[1,3,4], Biliana Nikolova[3], Shuhei Murayama[1], Desislava Lazarova[2], Iana Tsoneva[3] and Ichio Aoki[1]

[1] *Molecular Imaging Center, National Institute of Radiological Sciences, 4-9-1 Anagawa, Inage-ku, Chiba 263-8555, Japan*
[2] *Medical Faculty, Sofia University, 1 Koziak Str., Sofia 1407, Bulgaria*
[3] *Institute of Biophysics and Biomedical Engineering, Bulgarian Academy of Sciences, Sofia 1113, Bulgaria*
[4] *Medical Faculty, Trakia University, 11 Armeiska Str., Stara Zagora 6000, Bulgaria*

Abstract. The present study was designed to investigate whether poly-ion complex hollow vesicles (polymersomes), based on chemically-modified chitosan, are appropriate for lymph node mapping in the context of their application in the development of theranostic nanosized drug delivery systems (nano-DDS). The experiments were performed on Balb/c nude mice (colon cancer-grafted). The mice were subjected to anesthesia and quantum dot (QD^{705})-labeled polymersomes (d~120 nm) were injected intravenously *via* the tail vein. The optical imaging was carried out on Maestro EX Imaging System (excitation filter: 435–480 nm; emission filter: 700 nm). A strong fluorescent signal, corresponding to QD^{705} fluorescence, was detected in the lymph nodes, as well as in the tumor. A very weak fluorescent signal was found in the liver area. The half-life of QD^{705}-labelled polymersomes was 6 ± 2 hours in the bloodstream and 11 ± 3 hours in the lymph nodes. The data suggest that polymersomes are very promising carriers for lymph node mapping using QD as a contrast agent. They are useful matrix for development of nano-formulations with theranostic capabilities.

Key words: Polymersomes — Quantum dot — Lymph nodes — Imaging

Introduction

Lymph node targeting and mapping is a very important direction in the development of theranostic nanosized drug delivery systems (nano-DDS) due to the possibility to treat metastases and/or to visualize and remove the sentinel metastatic lymph nodes in surgery. The biopsy of the sentinel lymph nodes is very simple as a concept, but practically (technically) it is not so easy. In clinical practice, the most commonly used fluorophore for this purpose is isosulfan blue (Schaafsma et al. 2014). However, sometimes the sentinel lymph nodes could be located too deeply (to ~10 cm below the skin), which restricts their visualization and localization prior to surgery using conventional organic fluorophores. Therefore, each novelty in this methodology, that improves the technique, is accepted with a great enthusiasm by clinicians.

Correspondence to: Rumiana Bakalova, Molecular Imaging Center, National Institute of Radiological Sciences (NIRS), 4-9-1 Anagawa, Inage-ku, Choba 264-8555, Japan
E-mail: bakalova@nirs.go.jp

The fluorescent imaging using quantum dots (QDs) have a great potential for application in surgery – for a precise and fast localization of sentinel lymph nodes and small lesions (e.g., metastatic tumors), and facilitation of their removal. QDs allow visualization of the lymph nodes at a few centimeters below the skin surface, before proceeding to the resection. Thus, it is possible to reduce the size of the resection and to decrease the time of surgical intervention.

A lymph node mapping, using QDs, was first published in Nature Biotechnology (2004) by Bawendy and Frangioni's teams (Kim et al. 2004). Currently, there is no doubt about the clinical importance of this approach, especially in cancer therapy (Vahrmeijer et al. 2013). The near-infrared fluorescent nanoparticles have a real potential to replace the conventional organic fluorophores in the biopsy of the sentinel lymph nodes (Ashitate et al. 2014).

The selective disposition of nanocarriers into the target tissue is an essential issue in drug delivery and lymph node mapping. In the last several years, the critical size of nanocarriers (150 nm), discriminating the permeability into normal and tumor tissues, was determined by the use of size-tunable, polyion complex hollow vesicles (polymer-

somes) as a ruler (Meng et al. 2011; Bennett et al. 2014). Polymersomes are capable of encapsulating hydrophobic and hydrophilic drugs and they can be surface functionalized for target-selective drug delivery and delivery of imaging probes. Their polymeric membrane potentially offers a protective barrier to proteins, peptides, DNA and RNA fragments against deleterious factors that may be present in the biological environment (Bennett et al. 2014).

To evaluate the impact of polymersomes (made by different polymer matrices) as drug carriers, it is necessary to investigate their pharmacodynamics *in vivo* and especially the possibility to deliver them into the target tissues. One of the most preferred targets is cancer due to the efforts to develop highly specific therapeutic strategies with minimal side-effects. The polymersomes are usually labeled by different contrast agents and their pharmacodynamics in cancer and non-cancer tissues has investigated *in vivo* by optical imaging, magnetic resonance imaging, positron-emission tomography, multimodal imaging (Ghoroghchian et al. 2005; Duncan et al. 2008). Currently, a limited number of studied describe a localization of polymersomes (Tat-peptide or antigen-conjugated) in lymph nodes (Christian et al. 2009; Stano et al. 2013).

Semiconductor QDs are one of the most appropriate fluorescent markers for deep-tissue optical imaging of pharmacodynamics of polymersomes in living organisms (Kim et al. 2004; Bakalova et al. 2007). The unique optical properties of QDs can be used to optimize the signal-to-background ratio, to improve the sensitivity of fluorescence detection, and to increase the quality of fluorescent deep-tissue imaging *in vivo* (Kim et al. 2004; Bakalova et al. 2008). Moreover, single QDs can be observed and tracked for up to few hours by fluorescence confocal microscopy, total internal reflection microscopy, or basic wide-field epifluorescence microscopy, and single-molecule microscopy, as well as up to few days by optical (fluorescent) imaging systems. QDs are also excellent probes for two/multi-photon confocal microscopy because they are characterized by a large absorption cross-section (Bakalova et al. 2011; Osakada and Cui 2011; Chang and Rosenthal 2013; Hafian et al. 2014).

The present study was designed to investigate the possibility for lymph node mapping using QD-labeled size-controlled long-circulating polymersomes on experimental animals, visualized by fluorescent imaging *in vivo*, and to clarify their potential as a carrier of drugs and/or contrast agents in diagnostic and treatment of metastases.

Materials and Methods

Chemicals

Water-soluble polymersomes were prepared from cholanic acid-modified chitosan as it was described by Lee et al. (2012) – with slight modifications (QDs and saturated fatty acid were conjugated with chitosan, instead of siRNA). Labeling of polymersomes with QDs was carried out *via* carbodiimide chemistry, using N-(3-dimethylaminopropyl)-N‘-ethylcarbodiimide hydrochloride (EDC) as a zero-length cross-linker (Hermanson 1996). The nanoparticles were characterized by transmission electron microscopy (TEM), dynamic light scattering (DLS) and fluorescent spectroscopy. The concentration of QDs in polymersomes was calculated by the method of Yu et al. (2003). The structure of the nanoparticles and their physicochemical characteristics are shown in Scheme 1.

QDot®705 ITK™ Carboxyl Quantum Dots were purchased from Invitrogen. Isoflurane was purchased from

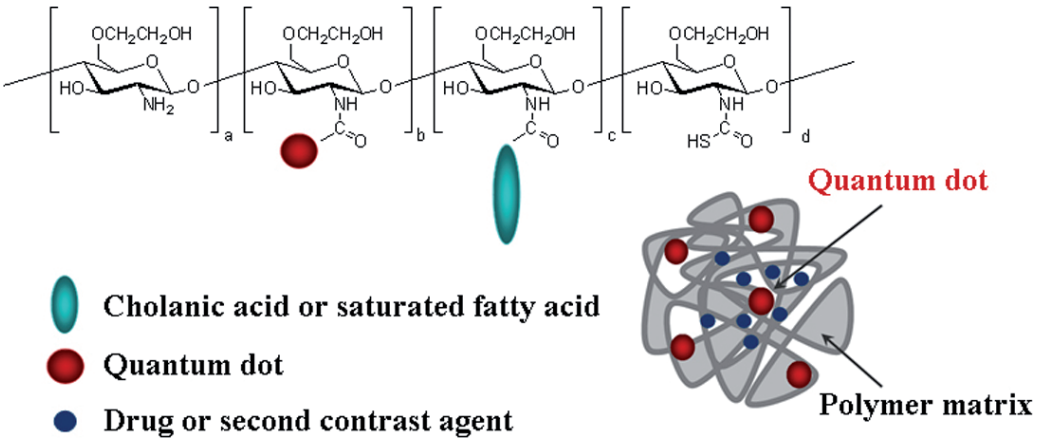

Scheme 1. Scheme and physicochemical characteristics of QD-labeled polymersomes, based on chemically modified chitosan. Physicochemical characteristics of QD-labeled polymersomes: average size – 128 nm; size-distribution ~30%; excellent water-solubility; stability in high-salt physiological fluids (aggregation was not detected).

Abbott (Japan). All chemicals used in this study were of analytical or HLPC grade.

Experimental cancer model

Balb/c nude mice (21 ± 2 g) were used. Conol26 cells (1×10^5 in 10 µl PBS, pH 7.4) were inoculated subdermally in the left/right hindpaw. All measurements were performed ~9–10 days after inoculation, when the tumour size was ~100 mm^3.

All experiments were conducted in accordance with the guidelines of the Physiological Society of Japan and were approved by the Animal Care and Use Committee of the National Institute of Radiological Sciences, Chiba, Japan.

Optical imaging

All experiments *in vivo* were conducted under anaesthesia. Briefly, the mouse was anaesthetized with 1.5% isoflurane using mask. The tail veil was catheterized for administration of nanoparticles and the mouse was fixed in the camera of the Maestro EX Imaging System, connected to anaesthesia device. The body autofluorescence was registered at excitation filter 435–480 nm and emission filter 700 nm (longpass). Nanoparticles (QD^{705} or QD^{705}-labelled polymersomes) were injected intravenously (i.v.) *via* the tail vain (single dose – 80 nmol; 100 µl volume) and the whole body fluorescence was registered on the back and stomach side at different

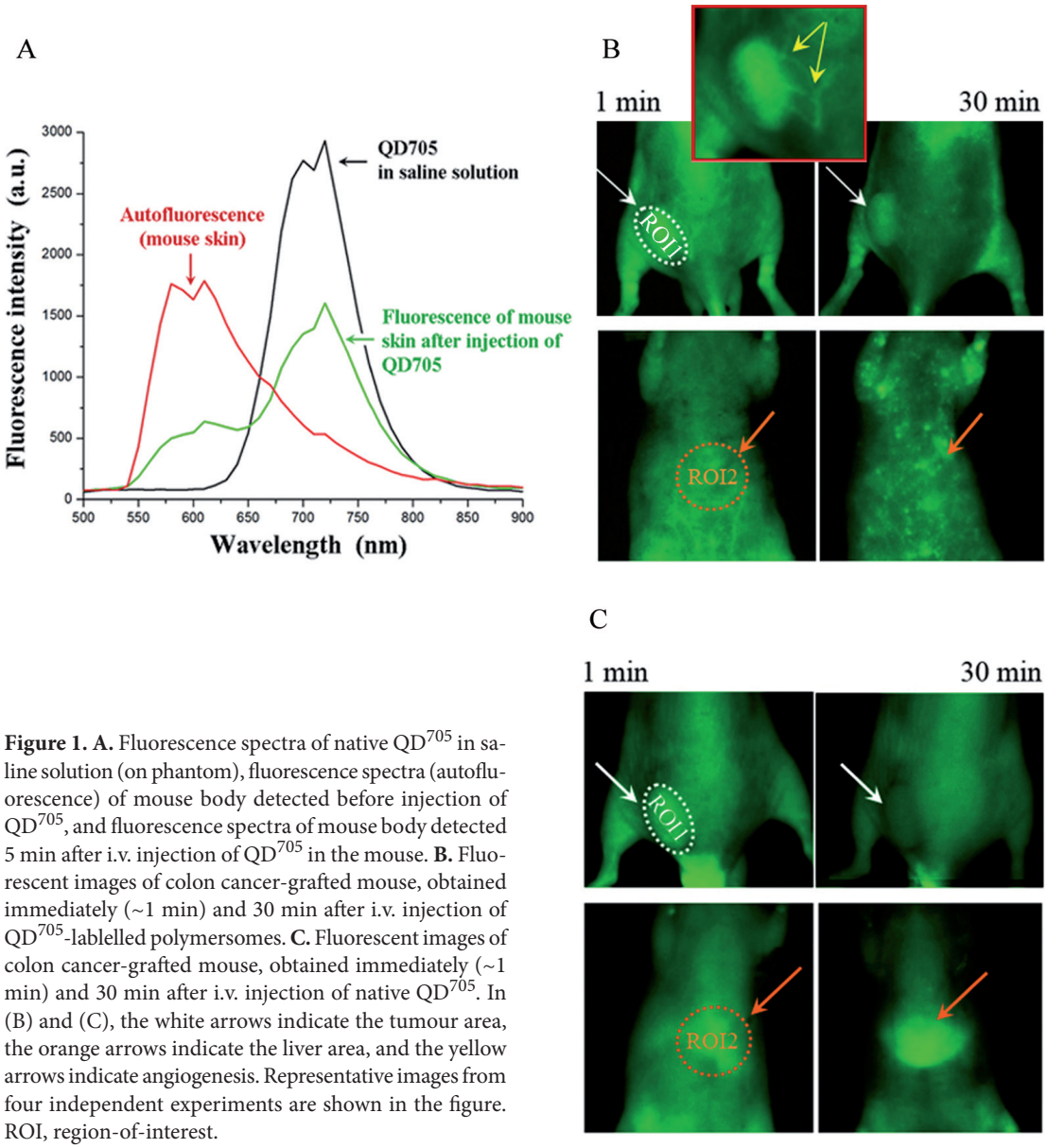

Figure 1. A. Fluorescence spectra of native QD^{705} in saline solution (on phantom), fluorescence spectra (autofluorescence) of mouse body detected before injection of QD^{705}, and fluorescence spectra of mouse body detected 5 min after i.v. injection of QD^{705} in the mouse. **B.** Fluorescent images of colon cancer-grafted mouse, obtained immediately (~1 min) and 30 min after i.v. injection of QD^{705}-lablelled polymersomes. **C.** Fluorescent images of colon cancer-grafted mouse, obtained immediately (~1 min) and 30 min after i.v. injection of native QD^{705}. In (B) and (C), the white arrows indicate the tumour area, the orange arrows indicate the liver area, and the yellow arrows indicate angiogenesis. Representative images from four independent experiments are shown in the figure. ROI, region-of-interest.

time-intervals. The data were analyzed by Living Image In Vivo Imaging software (Maestro version 2.10.0).

Results and Discussion

In preliminary experiment we selected the appropriate concentration of QD^{705} for *in vivo* imaging, which gives a high signal-to-background ratio without saturation of the fluorescent signal and existence of artifacts. Thus, before fluorescent imaging on cancer-grafted mice, all imaging parameters were optimized using native QD^{705} solutions in different concentrations, applied on phantoms and healthy mice (subcutaneous and intravenous injections in different volumes). The most optimal concentration of QD^{705} for *in vivo* application was a single dose of ~80 nmol in 100 µl volume.

Figure 1A shows the fluorescent spectra of native QD^{705} in saline solution (black line), autofluorescence spectra of mouse body (red line) and their overlap after injection of native QD^{705} in mouse *via* the tail vain (green line). The data indicate that QD^{705}, emitting in the near-infrared region of the spectrum (700–900 nm), allow to overcome the autofluorescence of mouse body and to obtain a strong fluorescent signal around 700–710 nm, which comes from the nanoparticles.

The images in Figure 1B,C were obtained on colon cancer-grafted mice, injected intravenously with QD^{705}-labelled polymersomes or native QD^{705} in a concentration, selected in preliminary experiments. The images were obtained immediately (~1 min) and 30 min after injection of the nanoparticles. In this short period after injection, the tumor was visualized on the basis of angiogenesis (yellow arrows) in both cases. The quantum yield of QD^{705} was high enough to allow a deep-tissue imaging of blood vessels. The native QD705 were rapidly accumulated into the liver, while QD^{705}-labelled polymersomes practically were not detected in the liver area.

Bright fluorescent spots were visualized on the stomach side of the mice, injected with QD-labelled polymersomes (Figure 2). In all overlapped spectra detected in these spots, there was a very well-defined fluorescent maximum

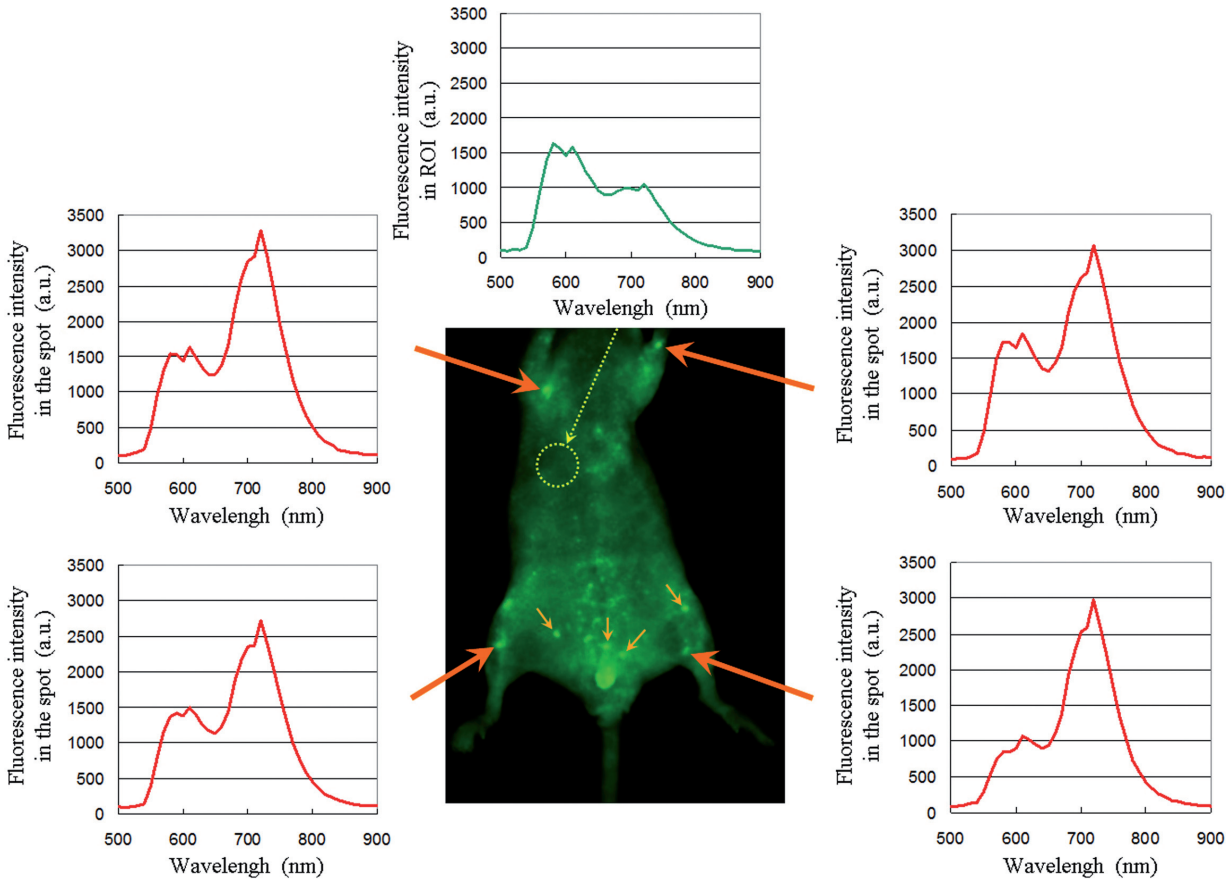

Figure 2. Visualization of lymph nodes in colon cancer-bearing mouse after i.v. injection of QD^{705}-labelled polymersomes. A representative image, obtained 30 min after injection is shown. The fluorescent spectra in red were obtained from each bright spot, indicated by orange arrows. The fluorescent spectrum in green was obtained from the region-of-interest (ROI), indicated by yellow dotted arrow.

at 705 nm, corresponding to the QD^{705}. The background spectrum (green line) detected outside the spots was characterized by a high maximum at ~600 nm and a comparatively small maximum at 705 nm. In situ imaging showed that these were lymph nodes (data are not shown).

The half-life of fluorescence intensity of QD^{705}-labelled polymersomes was 6 ± 2 hours in the bloodstream and 11 ± 3 hours in the lymph nodes. Maximum fluorescence intensity in the lymph nodes was detected on the 1st hours after injection, followed by a plateau within 3 hours and comparatively slow decrease within 3–24 hours (Figure 3). Weak fluorescent signal was detected in the liver area.

Recently, two teams only have reported a localization of size-controlled polymersomes (composed of different block copolymers) in lymph nodes. In 2009, Christian et al. have developed PZn_3-labeled Tat-peptide conjugated NIR-emissive polymersomes composed of poly(ethylene oxide (1300)-*b*-butadiene(2500)) with 4-fluoro-3-nitrobenzoic acid (Christian et al. 2009). The polymersomes have been applied for *in vivo* dendritic cell tracking using fluorescence lifetime imaging. During the measurements the authors have observed an accumulation of the fluorescent dye in the lymph nodes. In 2013, Stano et al. have described antigen-loaded polymersomes composed of poly(propylene sulfide) and poly(ethylene glycol) (Stano et al. 2013). The authors have observed that these nanoparticles induced enhanced frequencies of antigen-specific $CD4^+$ T cells in the spleen, lymph nodes and lungs. Our study is the first demonstrating a direct lymph node mapping using polymersomes conjugated with contrast agent (e.g., quantum dot).

The data suggest that size-controlled long-circulating polymersomes are very promising carriers for contrast substances in lymph node mapping and drug-carriers for treatment of metastases. They are useful matrix for development of nano-formulations with theranostic capabilities.

The growing number of studies on polymersomes shows that these nanoparticles are new and valuable tools for disease diagnosis and therapy. The enhanced stability and tunability of polymersomes will ultimately lead to the development of effective carriers for *in vivo* drug delivery, molecular imaging, and cellular mimicry. The potential to co-encapsulate two drug molecules in the same polymer-

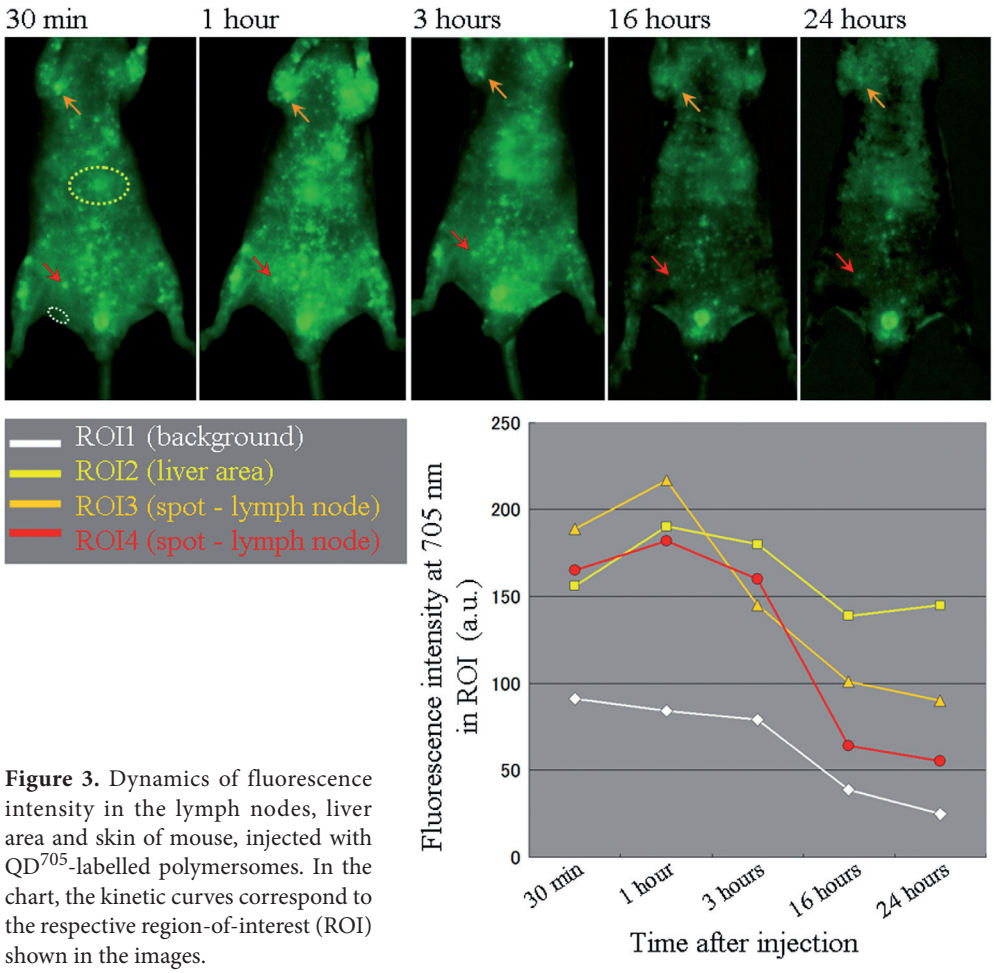

Figure 3. Dynamics of fluorescence intensity in the lymph nodes, liver area and skin of mouse, injected with QD^{705}-labelled polymersomes. In the chart, the kinetic curves correspond to the respective region-of-interest (ROI) shown in the images.

some enables combination therapies and eliminates the need to individually administer two separate drug formulations (Levine et al. 2008; Chen et al. 2014).

Acknowledgments. The authors thank Ms. Sayaka Shibata (Molecular Imaging Center, National Institute of Radiological Sciences, Japan) for her assistance during the experiments *in vivo*. This study was partially supported by a grant-in-aid „Kakenhi" (No. 24510321) from the Ministry of Education, Science and Technology of Japan (granted to R. B.) and JSPS Fellowship (granted to B. N.).

Conflict of interest. The authors report no conflicts of interest in this work.

References

Ashitate Y., Hyun H., Kim S. H., Lee J. H., Henary M., Frangioni J. V., Choi H. S. (2014): Simultaneous mapping of pan and sentinel lymph nodes for real-time image-guided surgery. Theranostics **4,** 693–700
http://dx.doi.org/10.7150/thno.8721

Bakalova R., Zhelev Z., Aoki I., Kanno I. (2007): Designing quantum dot probes. Nat. Photonics **1,** 487–489
http://dx.doi.org/10.1038/nphoton.2007.150

Bakalova R., Zhelev Z., Gadjeva V. (2008): Quantum dots versus organic fluorophores in fluorescent deep-tissue imaging – merits and demerits. Gen. Physiol. Biophys. **27,** 231–242

Bakalova R., Zhelev Z., Kokuryo D., Spasov L., Aoki I., Saga T. (2011): Chemical nature and structure of organic coating of quantum dots is crucial for their application in imaging diagnostics. Int. J. Nanomedicine **6,** 1719–1732
http://dx.doi.org/10.2147/IJN.S17995

Bennett K. M., Jo J., Cabral H., Bakalova R., Aoki I. (2014): MR imaging techniques for nano-pathophysiology and theranostics. Adv. Drug Deliv. Rev. **74,** 75–94
http://dx.doi.org/10.1016/j.addr.2014.04.007

Chang J. C., Rosenthal S. J. (2013): Quantum dot-based single-molecule microscopy for the study of protein dynamics. Methods Mol. Biol. **1026,** 71–84
http://dx.doi.org/10.1007/978-1-62703-468-5_6

Chen W., Meng F., Cheng R., Deng C., Feijen J., Zhong Z. (2014): Advanced drug and gene delivery systems based on functional biodegradable polycarbonates and copolymers. J. Control. Release **190,** 398–414
http://dx.doi.org/10.1016/j.jconrel.2014.05.023

Christian N. A., Benencia F., Milone M. C., Li G., Frail P. R., Therien M. J., Coukos G., Hammer D. A. (2009): In vivo dendritic cell tracking using fluorescence lifetime imaging and near-infrared-emissive polymersomes. Mol. Imaging Biol. **11,** 167–177
http://dx.doi.org/10.1007/s11307-008-0184-x

Duncan T. V., Ghoroghchian P. P., Rubstov I. V., Hammer D. A., Therien M. J. (2008): Ultrafast excited-state dynamics of nanoscale near-infrared emissive polymersomes. J. Am. Chem. Soc. **130,** 9773–9784
http://dx.doi.org/10.1021/ja711497w

Ghoroghchian P. P., Frail P. R., Susumi K., Blessington D., Brannan A. K., Bates F. S., Chance B., Hammer D. A., Therien M. J. (2005): Near-infrared-emissive polymersomes: self-assembled soft matter for in vivo optical imaging. Proc. Natl. Acad. Sci. USA **102,** 2922–2977
http://dx.doi.org/10.1073/pnas.0409394102

Hafian H., Sukhanova A., Turini M., Chames P., Baty D., Pluot M., Cohen J. H., Nabiev I., Millot J. M. (2014): Multiphoton imaging of tumour biomarkers with conjugates of single-domain antibodies and quantum dots. Nanomedicine **10,** 1701–1709
http://dx.doi.org/10.1016/j.nano.2014.05.014

Hermanson G. T. (1996): Bioconjugate Techniques. Academic Press, New York

Kim S., Lim Y. T., Soltesz E. G., De Grand A. M., Lee J., Nakayama A., Parker J. A., Mihaljevic T., Laurence R. G., Dor D. M., et al. (2004): Near-infrared fluorescent type II quantum dots for sentinel lymph node mapping. Nat. Biotechnol. **22,** 93–97
http://dx.doi.org/10.1038/nbt920

Lee S. J., Huh M. S., Lee S. Y., Min S., Lee S., Koo H., Chu J.-U., Lee K. E., Jeon H., Choi Y., et al. (2012): Tumor-homing poly-siRNA/glycol chitosan self-cross-linked nanoparticles for systemic siRNA delivery in cancer treatment. Angew. Chem. Int. Ed. Engl. **51,** 7203–7207
http://dx.doi.org/10.1002/anie.201201390

Levine D. H., Ghoroghchian P. P., Freudenberg J., Zhang G., Therien M. J., Greene M. I., Hammer D. A., Murali R. (2008): Polymersomes: A new multi-functional tool for cancer diagnosis and therapy. Methods **46,** 25–32
http://dx.doi.org/10.1016/j.ymeth.2008.05.006

Meng H., Xue M., Xia T., Ji Z., Tarn D. Y., Zink J. I., Nel A. E. (2011): Use of size and a copolymer design feature to improve the biodistribution and the enhanced permeability and retention effect of doxorubicin-loaded mesoporous silica nanoparticles in a murine xenograft tumor model. ACS Nano **5,** 4131–4144
http://dx.doi.org/10.1021/nn200809t

Osakada Y., Cui B. (2011): Real-time visualization of axonal transport in neurons. Methods Mol. Biol. **670,** 231-243
http://dx.doi.org/10.1007/978-1-60761-744-0_16

Schaafsma B. E., Verbeek F. P., Elzevier H. W., Tummers Q. R., van der Vorst J. R., Frangioni J. V., van de Velde C. J., Pelger R. C., Vahrmeijer A. L. (2014): Optimization of senthinel lymph node mapping in bludder cancer using near-infrared fluorescence imaging. J. Surg. Oncol. **110,** 845–850
http://dx.doi.org/10.1002/jso.23740

Stano A., Scott E. A., Dane K. Y., Swartz M. A., Hubell J. A. (2013): Tunable T cell immunity towards a protein antigen using polymersomes vs. solid-core nanoparticles. Biomaterials **34,** 4339–4346
http://dx.doi.org/10.1016/j.biomaterials.2013.02.024

Yu W. W., Qu L., Guo W., Peng X. (2003): Experimental determination of the extinction coefficient of CdTe, CdSe, and CdS nanocrystals. Chem. Mater. **15,** 2854–2860
http://dx.doi.org/10.1021/cm034081k

Vahrmeijer A. L., Hutteman M., van der Vorst J. R., van de Velde C. J., Frangioni J. V. (2013): Image-guided cancer surgery using near-infrared fluorescence. Nat. Rev. Clin. Oncol. **10,** 507–518
http://dx.doi.org/10.1038/nrclinonc.2013.123

Received: December 2, 2014
Final version accepted: February 20, 2015
First published online: July 29, 2015